Nonlinear Dynamics (2026) 114:131
https://doi.org/10.1007/s11071-025-11996-2

RESEARCH

Statistical laws of banded vegetation patterns in heterogeneous environments

Eduardo A. Droguett-Mora[1] · Belén Hidalgo-Ogalde[1] · Marcel G. Clerc[1] · Mustapha Tlidi[2]

Received: 19 August 2025 / Revised: 1 October 2025 / Accepted: 18 October 2025

Abstract
Large-scale banded vegetation patterns are a well-documented phenomenon in many semi-arid ecosystems. Most theoretical efforts have focused on understanding spatially regular patterns; however, field observations reveal that the spatial distribution of vegetation is often irregular. The laws governing these patterns remain unknown. We show through remote sensing data analysis that the width of the bands that constitute the vegetation patterns obeys a q-Gaussian distribution. Likewise, the spectral density of the vegetation patterns follows an exponential-law decay at sub-wavelengths. These results do not depend on the type of plants nor the type of soil, and can be observed across different landscapes. Furthermore, the observations are reproduced by employing a fully deterministic model for the biomass. Our results reveal the statistical laws that govern the irregularities in banded vegetation patterns.

Keywords Pattern formation · Population dynamics · Vegetation patterns · Spatiotemporal chaos

1 Introduction

In arid and semi-arid landscapes, plant communities often show a non-uniform spatial distribution at centimeter, meter, or even hectometer scales. An interesting example of botanical organization, generically referred to as vegetation patterns, is the tiger bush [1]. This phenomenon is particularly evident in semi-arid and arid landscapes where the evapotranspiration potential is significantly higher than the average annual rainfall, and/or in nutrient-poor environments. At the level of the individual plant, water stress affects both survival and growth. At the community level, it favors clustering behavior, leading to landscape fragmentation. It is generally accepted that this adaptation to hydric stress involves a symmetry-breaking instability [2–6]. These spatial distributions are mostly studied by mathematical models that yield regular, or ideal patterns. Even though field observations reveal irregularities, these are usually not taken into account, and the laws governing them are still unknown. To clarify the irregularities of patterns, several concepts have been proposed [7–9], including *extreme irregularity* and a scale-free regime, which both refer to entirely irregular patterns. *Intermediate regularity*, on the other hand, is characterized by patterns that exhibit specific correlations along with significant fluctuations in their correlograms and periograms. *Regular* or *perfect* patterns show clear correlations without fluctuations in their correlograms and periograms.

Pattern irregularities arise from the non-reciprocity and non-locality of the interactions, and not as a consequence of noise or random fluctuations. The interaction of different components of a given system can be reciprocal or non-reciprocal. Non-reciprocal coupling refers to a phenomenon in which the interaction between two parts of a system depends on the direction of the interaction. In other words, the energy transferred from one region to another may differ compared to the energy transferred back from the latter region to the former. A wide variety of physical phenomena are well described by non-reciprocal interaction in far-from-equilibrium systems, such as biology [10], optics [11–14], acoustics [15], metamaterials [16, 17] and liquid crystals [18]. In all these systems, despite their origins, the absence of reciprocity is the rule rather than the exception. The interaction is non-reciprocal when the exchange of its components does not produce an equivalent result. In plant

✉ Eduardo A. Droguett-Mora
eduardo.droguett@ug.uchile.cl

[1] Departamento de Física and Millennium Institute for Research in Optics, Facultad de Ciencias Físicas y Matemáticas, Universidad de Chile, Casilla 487-3, Santiago, Chile

[2] Département de Physique, Faculté des Sciences, Université Libre de Bruxelles (U.L.B.), CP 231, Campus Plaine, B-1050 Bruxelles, Belgium

Published online: 20 January 2026

ecology, the non-reciprocity in the interactions arises from the environmental anisotropies, such as slope, wind, soil depth distribution, and soil-moisture islands. These can modify the pattern wavelength and symmetry. In the last decades, the effect of anisotropy on vegetation patterns has been of great interest [2, 3, 19–21]. The wavelength as well as the speed of uphill banded vegetation have been estimated [22]. In contrast, in hyper-arid ecosystems such as fog deserts, the banded vegetation moves downhill [19]. The wavelength of the banded vegetation pattern is directly proportional to the degree of drought, but varies negatively with the slope gradient [23].

The stochastic approach highlights the potentially structuring role of environmental randomness, considered as a source of symmetry-breaking transitions induced by noise, which can trigger the formation of vegetation patterns [24, 25]. These transitions occur when the variance of environmental noise increases, while its mean value remains constant. Stochastic fluctuations–whether in time [26] or space [27]–can profoundly influence the stability of nonlinear systems. These fluctuations may arise from various sources and can be classified as either additive (internal) or multiplicative (external) noise. Their origins are diverse, including topographical irregularities, heterogeneous soil properties, and random seed dispersal. The growing interest in the impact of stochastic processes on the formation of vegetation patterns is evident from the large number of recent scientific publications on the subject [28–34]. In particular, persistent spatial noise over time represents a form of exogenous heterogeneity, often referred to as geodiversity [9, 35, 36]. Further, regular natural vegetation patterns differ fundamentally from periodic patterns, not because of superimposed noise [37], but because of intrinsic variations in size, spacing, and frequency, as demonstrated by Kästner et al. [7] using statistical analyses on a large data set [8]. This challenges the common assumption that dislocation dynamics are merely transient. Moreover, certain regimes are predicted to exhibit a stable spatial distribution of defects [38].

This letter aims to show that the spatial irregularities presented in intermediate regular banded vegetation patterns follow a q-Gaussian distribution [39, 40], characterized by power-law tails $L^{-2/(q-1)}$ where L is the vegetation bandwidth. Figure 1 shows a single vegetation band statistic of width L. To figure out the origin of the power law in vegetation bandwidth distribution, we analyze via remote sensing imaging the ground covered by vegetation. This technique has been used in previous studies [19, 23, 38], and it serves as an estimate of the biomass [41]. Specifically, we study the spectral density of the biomass and its orientation field. The spectral density of the biomass exhibits an exponential-law decay, while the biomass orientation field shows a power law decay with an exponent close to 2, both in the sub-wavelength regime. Theoretically, a fully deterministic model based on non-local facilitative and competitive non-reciprocal interactions explains the field observations qualitatively.

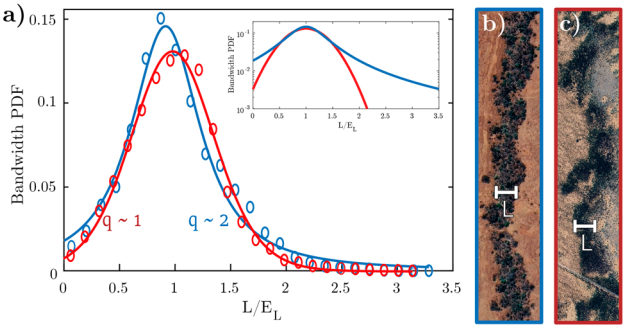

Fig. 1 Statistics of single vegetation bandwidths. **a** Probability distribution function (PDF) of vegetation bandwidths L. Blue and red curve account for the q-Gaussian and Gaussian distribution, respectively. Blue and red points represent the data obtained in Sudan (011°09'00.00"N 028°16'30.00"E) and in Mexico (028°08'30.00"N 104°28'00.00"W). Inset stands for the same width distributions on a logarithmic vertical axis. Remote image of a vegetation band **b** in Sudan and **c** in Mexico

2 Remote sensing image analysis

Most striped vegetation patterns observed in nature are disordered and exhibit topological defects such as dislocations. In addition to slope, which promotes the propagation of these dislocations, boundary conditions have been shown to play a key role in their ongoing creation [38]. This permanent dynamics with previous studies that considered dislocation formation to be a transient phenomenon, ultimately leading to perfectly ordered, defect-free patterns [3, 43]. Banded vegetation patterns are formed in arid- and semi-arid landscapes as a result of an interplay between short-range facilitative interactions controlling plant reproduction and long-range inhibition interactions caused by plant competition for scarce resources.

When the environmental conditions are heterogeneous, banded vegetation patterns become irregular. Figures 2(a) and 2(b) show two examples of large spatial scales banded vegetation patterns with irregular spatial distributions and an average wavelength λ. The probability density functions (PDFs) for the bandwidths are shown in Figs. 2(c) and 2(d). Note that, given each band, the width L is calculated at each position along the band. The probability density functions represent the frequency distribution of different bandwidths observed in Chilean and Sudanese landscapes, respectively. This is an invaluable tool for analyzing spatial patterns and understanding the distribution of certain features within ecosystems. Figure 2(c) shows that the expectation and the average values coincide for the Sudanese vegetation. The blue dots and curves show a q-Gaussian distribution that fits with $q \approx 2$. Table 1 summarizes the q parameters of the

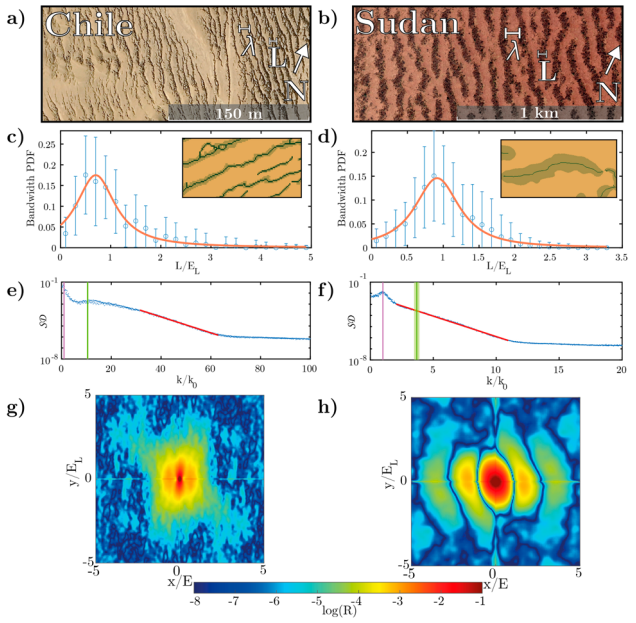

Fig. 2 Banded vegetation patterns and their statistical characterization. The left and right columns account for the Chilean and Sudanese landscapes. The white arrow points north. **a** Satellite image of Chile (020°29'30.00"S 070°03'30.00"W). **b** Satellite image of Sudan (011°09'00.00"N 028°16'30.00"E). **c** and **d** Histogram of the bandwidths (normalized by the expectation value) projected along the average direction of the pattern. Blue dots are the probability of the observed bandwidth. Error bars account for the standard deviation. Orange curves correspond to q-Gaussian fitting to the bandwidth distribution. Insets account for the skeleton (dark green curves) and binarization (shadowed light green band) of the respective landscape zoom. **e** and **f** Spectral density $\mathcal{SD}$ of the bands projected along the average direction of the pattern. The shadowed green regions account for the width variance. The vertical purple line accounts for the pattern wavelength λ. The green vertical line indicates the expectation value of the bandwidth. The green shaded areas account for the variance in width. **g** and **f** are the autocorrelation functions of the biomass. The images are obtained from Google Earth, using the *save image* tool, in Max. resolution (8192 × 7016 pixels) [42]

q-Gaussian distributions for several landscapes with their respective perceptual error of skewness (ε_s) and kurtosis (ε_k). These errors account for the difference of the distributions in terms of their asymmetry and asymptotic tails, respectively. We have considered other distributions, such as the Gamma or Weibull distributions, but the one that best represents the observed distribution is the q-Gaussian distribution (cf. Appendix B). This last distribution can be understood as a generalization of Gaussian distributions, which typically account for stochastic phenomena by including long-range correlations induced by dominant deterministic effects [39, 40]. Table 1 also shows the degree of exogenous spatial heterogeneity relative to the mean, the coefficient of variation CV [9]. We then compute the average spectral density of the biomass b, $\mathcal{SD} = \langle |\mathcal{F}[b - \bar{b}]|^2 \rangle / \mathcal{N}$ where $\mathcal{F}$ is the Fourier transform, k is the wavenumber along the average orientation of the pattern, $\bar{b}$ is the mean biomass of each image, $\langle \cdot \rangle$ is the average along the orthogonal mean orientation of the pattern, and $\mathcal{N}$ is a normalization factor that allowed for the scattered spectral density to be interpreted as a probability density function. Note that this normalization allows one to compute the Shannon entropy $H = -\sum_k p(k) \log[p(k)]$ of the spectral density, giving information of the complex spatial distribution of the different landscapes. Table 1 summarizes the estimated entropy values for the different regions studied. This allows us to characterize the most ordered and disordered regions, respectively. On the other hand, the maximum of the spectral density is also a measure of complexity; for sharper peaks, one has a more regular pattern, and for flattened distributions, one has more irregular patterns. The biomass b was estimated by the greyscale intensity of the superficial landscape images. The results are shown in Figs. 2(e) and 2(f). Both ecosystems clearly show a exponential law decay at large wavenumber e^{-mk} ($m \sim 0.17$ and $m \sim 0.85$ for Chile and Sudan, respectively), i.e., sub-wavelength. The green shaded regions account for the variance in bandwidth. Note that this type of exponential behavior is a manifestation of chaotic dynamics [44, 45]; however, it does not involve a large number of spatial modes.

A traditional way to characterize the organization of patterns and the degree of disorder is by calculating their autocorrelation. Figures 2(g) and 2(h) show the autocorrelation functions or correlograms of the biomass. These figures indicate the orientation of the pattern and the level of disorganization present. The images appear powdery, suggesting that the more powdery the image, the greater the disorder in the pattern.

Figure 3 summarizes the spectral density of the banded irregular patterns around the world. We investigated seven semi-arid and arid regions around the world, adding around 174 square kilometers of previously reported patterns on diverse continents. The selected patterns manifest bands with a preferred orientation. Indeed, all spectral densities have similar exponential-law decays. In addition, table 1 also summarizes the pattern wavelength λ, expectation value E_L, exponential law exponents m and distribution entropy H. Likewise, the histogram of the bandwidths follows q-Gaussian distributions with exponents q varying between 1 and 2. The respective correlograms of the different regions under study are presented in Appendix E. Hence, the self-organization process at sub-wavelengths leading to intermediate regular banded vegetation patterns is a universal feature in arid and semi-arid landscapes.

To shed more light on the spatial irregularity of the banded vegetation patterns, we investigate the pattern orientation field $\Phi(\vec{r})$ of the biomass [46]. This orientation field provides information about the complex irregularity of the pattern, and it corresponds to the local orientation of the pattern with respect to a given direction (see Fig. 4). For more details

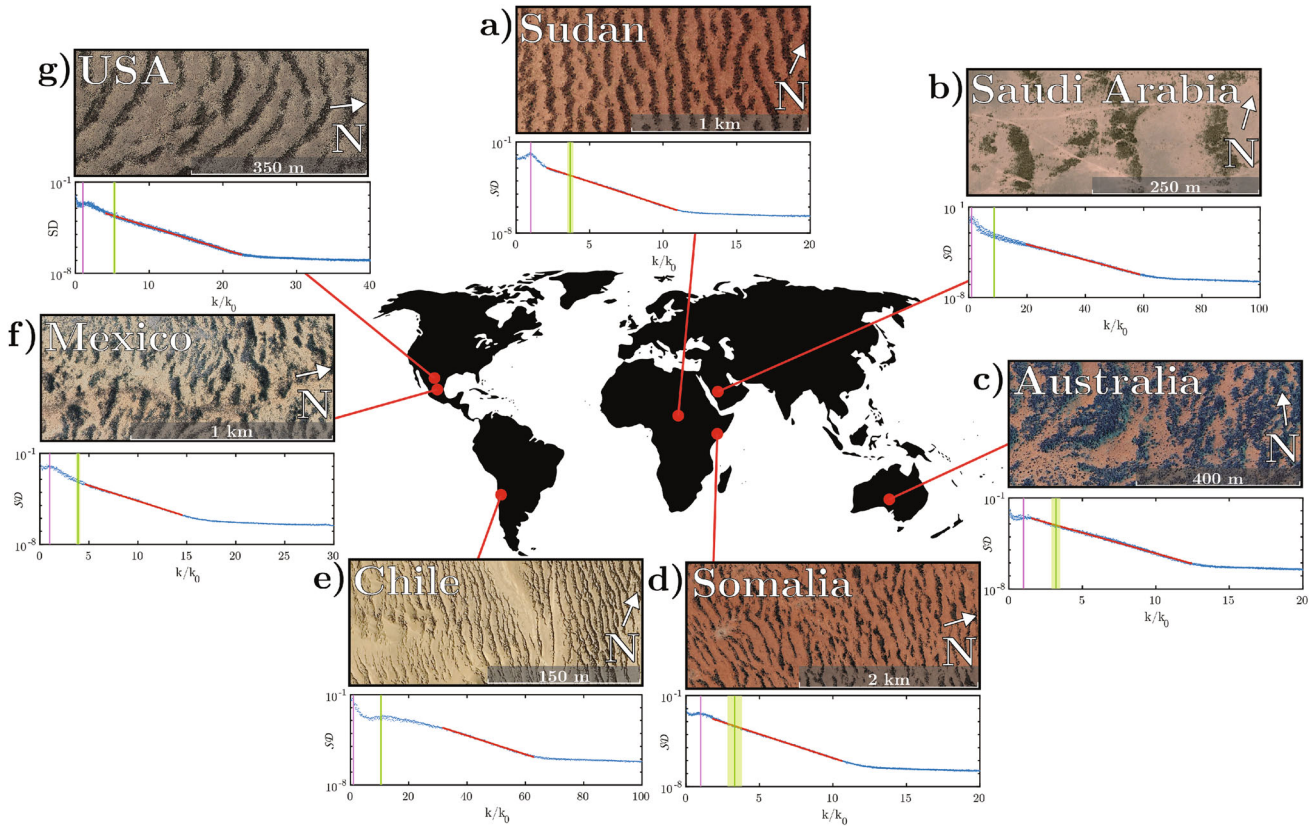

Fig. 3 Landscape images and spectral density of intermediate regular vegetation patterns in four continents: **a** Sudan (011°09'00.00"N 028°16'30.00"E), **b** Saudi Arabia (024°19'48.00"N 042°55'12.00"E), **c** Australia (023°23'41.67"S 133°22'53.99"E), **d** Somalia (008°06'54.00"N 047°26'30.00"E), **e** Chile (020°29'30.00"S 070°03'30.00"W), **f** Mexico (028°08'30.00"N 104°28'00.00"W), and **g** USA (031°02'30.00"N 103°05'30.00"W). The white arrow points north. The purple and green vertical line indicates the pattern characteristic wavenumber and the expectation value of the bandwidth. The green shaded areas account for the variance in width.

Table 1 Intermediate regular vegetation banded patterns and their statistical characterization values. The first column is the studied landscape. The second column is the total area analyzed per region. The third column is the coefficient of variation of the bandwidths (CV). q is the fitted q-parameter for the q-Gaussian distribution, with the uncertainty being the 95% interval. ε_s, ε_k are the percentual skewness and kurtosis errors of the fit. The seventh column is the average pattern wavelength λ. E_L is the expectation value for the bandwidths. The ninth column is the exponential law decay exponent m for the biomass spectral density, and m_o is the power law decay exponent of the biomass orientation field. H is the entropy of the spectral density distribution

Region	Area (km^2)	CV	q	ε_s (%)	ε_k (%)	λ (meters)	E_L/λ	m	m_o	H
Australia	21.2	0.57	1.4 ± 0.2	2.7	0.5	73	0.32	0.73	2.28	0.71
Chile	0.6	0.68	2.0 ± 0.5	2.5	2.6	6	0.14	0.17	2.21	0.59
Mexico	23.5	0.42	1.2 ± 0.2	5.3	1.9	101	0.25	0.55	2.79	0.65
Saudi Arabia	5.1	0.68	1.6 ± 0.4	6.8	11.9	37	0.22	0.14	2.29	0.61
Somalia	86.8	0.45	1.4 ± 0.1	2.6	2.9	248	0.21	0.85	1.95	0.69
Sudan	25.5	0.44	1.8 ± 0.3	2.1	3.0	93	0.31	0.85	1.93	0.64
USA	11.0	0.46	1.6 ± 0.3	7.2	5.1	55	0.37	0.40	1.89	0.70

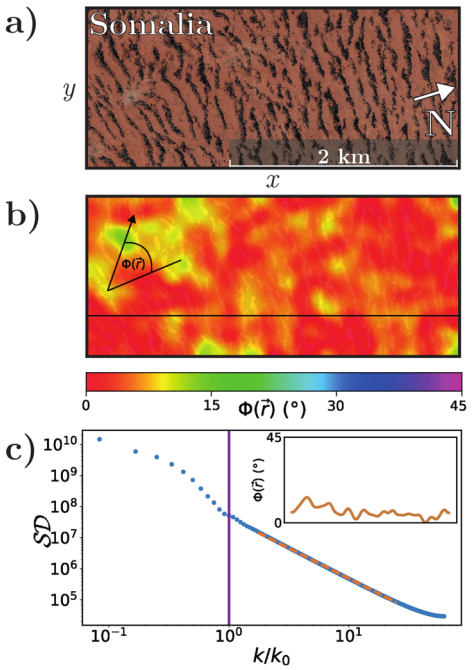

Fig. 4 Orientation field of the banded vegetation patterns. **a** Satellite image of a banded vegetation pattern in Somalia (008°06'54.00"N 047°26'30.00"E). The white arrow points north. **b** Orientation field Φ of the pattern. The black line indicates the location of the cut obtained for the inset in **c**. **c** Spectral density $\mathcal{SD}$ of the orientation field. The purple vertical line shows the pattern characteristic wavenumber. Inset: profile of the orientational field along the black line

on the orientation field, see Appendix C. An example of a vegetation pattern and its orientation field for a Somali landscape is shown in Figs. 4(a) and 4(b). The spectral density of the orientation field $\Phi(\vec{r})$ along the average direction of the pattern is shown in Fig. 4(c). From this chart, one can infer that the vegetation pattern orientation field is influenced by a power law decay k^{-m_o} with an exponent of approximately $m_o = 2$. Analogously, we perform this analysis for the previously reported landscapes. This analysis suggests that the power law decay of the vegetation orientation field is universal, as shown in figure 5 and table 1.

In brief, we show that the complex irregularity of banded vegetation patterns follows a q-Gaussian distribution. The banded vegetation patterns are also characterized by a spectral density of the biomass with an exponential-law decay and pattern orientation field with a power law decay, both in the sub-wavelengths.

3 Theoretical modeling

We incorporate non-reciprocal effects in the interaction redistribution model, where the spatial distribution of all plants is described by a single global variable $b = b(\mathbf{r}, t)$. This biomass density at time t and point $\mathbf{r} = (x, y)$ is defined as the plant biomass per unit area, with (x, y) being the two-dimensional space of Cartesian coordinates defined at the ground surface. We keep the mathematical structure of the interaction redistribution model [4]

$$\partial_t b = b(1-b)M_f[b] - \mu b M_c[b] + D\nabla^2 b. \tag{1}$$

The first and second terms of the right-hand side of the model Eq. (1) describe two opposing feedbacks: enhancement and decay of vegetation growth. The last term models the seed dispersion or vegetation encroachment, which is assumed to be described by a simple random walk diffusive process. The parameters μ and D account for the level of aridity and diffusion coefficient. Due to the time scale difference between the biomass dynamics and the environmental seasonality, an adiabatic elimination can be performed, and these parameters remain constant in time. M_f and M_c are functionals of biomass describing the non-local and nonlinear facilitation and competition feedback, respectively. Their mathematical expressions are

$$M_i[b](\mathbf{r}) = \exp\left[\chi_i \int \mathcal{K}_i(\mathbf{r}-\mathbf{r}')b(\mathbf{r}')d\mathbf{r}'\right],$$

with the subscript $i = \{f, c\}$ represents facilitative (f) and competitive (c) feedback. χ_i are the strengths of the interactions.

The time scale associated with Eq. (1) is inversely proportional to the vegetation growth rate and approximately corresponds to the time required for dominant trees to reach maturity, estimated at around ten years. The formation of two-dimensional localized structures typically occurs over 100 to 1,000 dimensionless time units, which translates to a real-world timespan of 100 to 1,000 years. Over such long periods, environmental conditions–such as rainfall, temperature, light, and wind–can be considered relatively stable on average. The spatial scale of local vegetation-water models is based on explicit water dynamics and local feedback between vegetation and water availability. In contrast, the interaction-redistribution model distills hydrological processes, emphasizing non-local interactions between plants, such as competition and facilitation. This model uses biomass redistribution to explain pattern formation, without needing to include hydrological variables in the modeling.

Such botanical self-organization is not limited to a specific type of plant [47]; it can involve grasses, shrubs, or trees. Furthermore, its occurrence is not restricted to a specific soil type, as it has been documented across a broad spectrum of soil types, encompassing sandy [48], silty [49], and clayey soil [2]. It is important to note that, while the results are consistent with observations, they do not serve as formal evidence of causality. Additionally, the model parameters were not specifically calibrated to account for local atmospheric

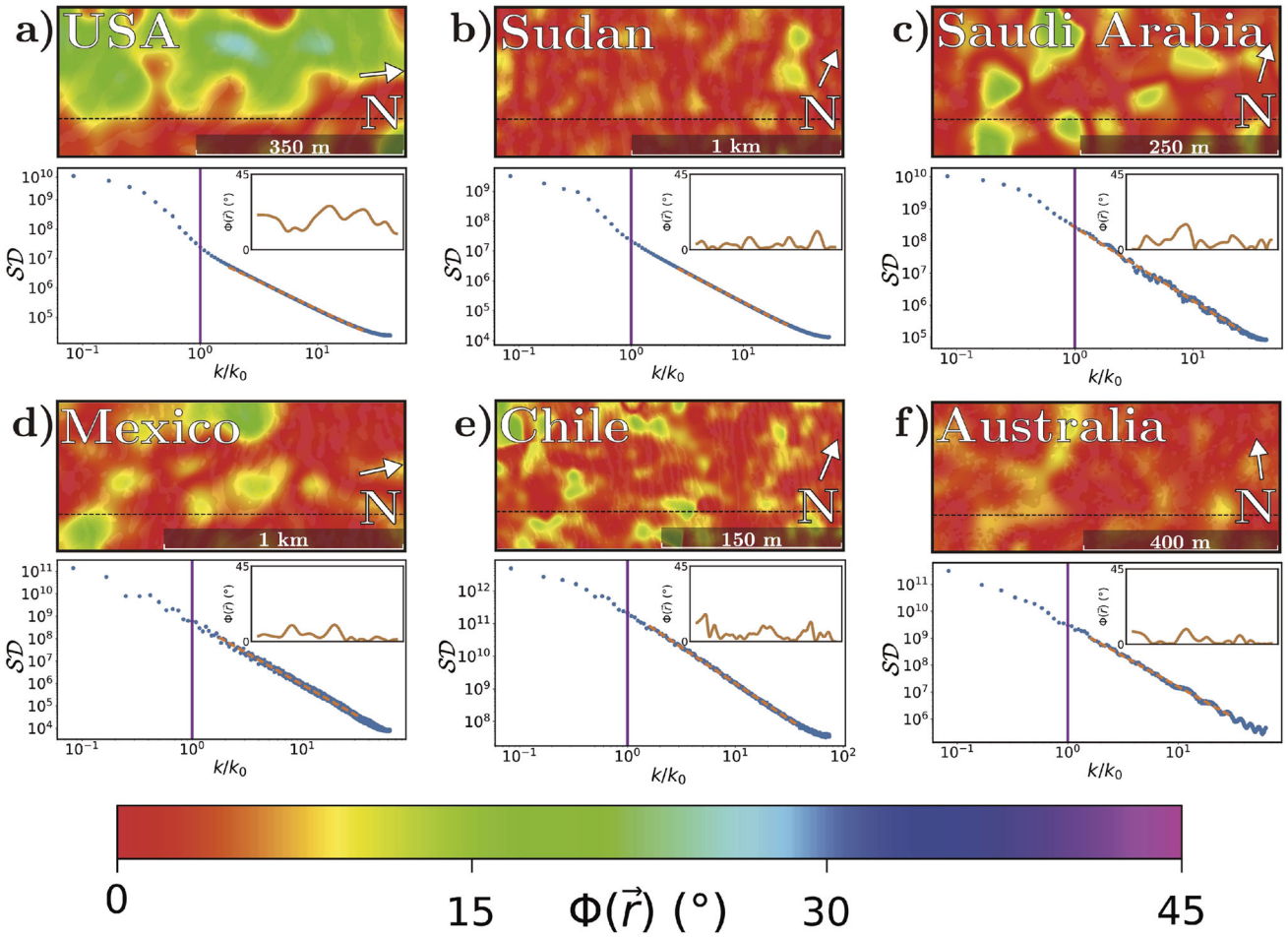

Fig. 5 Orientation field Φ and its spectral density $\mathcal{SD}$ of banded vegetation patterns in four continents: **a** USA (031°02'30.00"N 103°05'30.00"W), **b** Sudan (011°09'00.00"N 028°16'30.00"E), **c** Saudi Arabia (024°19'48.00"N 042°55'12.00"E), **d** Mexico (028°08'30.00"N 104°28'00.00"W), **e** Chile (020°29'30.00"S 070°03'30.00"W), and **f** Australia (023°23'41.67"S 133°22'53.99"E). The white arrow points north. The purple vertical line shows the pattern characteristic wavenumber

or topographic conditions. Other factors, such as topography, soil variability, or climatic effects, may also play a role in the formation of patterns. Therefore, the results obtained from model Eq. (1) are qualitative and general in nature.

When the environmental conditions are uniform, the system is isotropic and both facilitation and competition kernels $\mathcal{K}_i$ preserve the reflection symmetry $\mathbf{r} \to -\mathbf{r}$ and symmetry rotations. Hence, the kernels are even functions. For the sake of simplicity, we consider Gaussian kernels, $\mathcal{K}_i = \exp[-(x^2+y^2)]/2\pi l_i^2$. The range of the facilitative (competitive) non-local interaction is denoted by $l_f(l_c)$. Figure 6(a) depicts the isotropic environmental conditions. In this case, the system selects the spatial symmetry of the pattern and orientation. In general, the patterns are motionless. The positive feedback operates over a distance l_f of the order of the plant aerial structures, i.e., the radius of the crown or the canopy, as shown in Fig. 6(a). It involves, in particular, a reciprocal sheltering of neighboring plants against adverse conditions. The negative feedback is described by non-local competitive interaction between individual plants for the scarce resources, such as water and nutrients. For patterns to form, competition interactions must be of longer range than facilitation interactions [2] [cf. Fig. 6(a)]

The situation that interests us requires that the environmental conditions are not isotropic. Anisotropy is caused by atmospheric factors such as dominant wind and sunlight, or geomorphic effects such as topography, soil depth distribution, and soil-moisture islands. In these landscapes, the Gaussian kernel becomes

$$\mathcal{K}_i(\mathbf{r}) = \frac{1}{2\pi l_{ix} l_{iy}} \exp\left[-\frac{(x-a_i)^2}{2l_{ix}^2} - \frac{(y-b_i)^2}{2l_{iy}^2}\right]. \qquad (2)$$

Anisotropy introduced in the model Eq. (1) at the level of the kernel breaks the reflection ($\mathbf{r} \nrightarrow -\mathbf{r}$) and rotational symmetry. The simplest way of achieving this is by translating

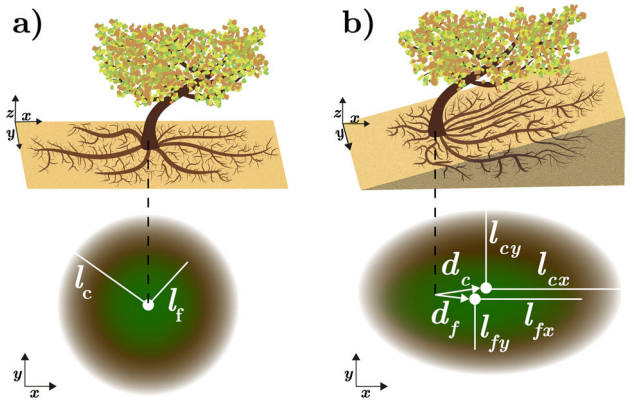

Fig. 6 Schematic representation of a tree in an arid landscape and the associated facilitation-competition, non-local and non-reciprocal interactions in (**a**) isotropic and (**b**) anisotropic environmental conditions. l_f, and l_c, are the range of the facilitative and competitive reciprocal non-local interaction, respectively. The vertical dashed lines stand for the position of the tree. l_{fx}, and l_{fy}, (l_{cx}, and l_{cy}) are the range of the non-reciprocal and non-local facilitative (competitive) along the x and y direction, respectively. The vectors $\mathbf{d}_f$ and $\mathbf{d}_c$ shift the origin of the kernels, associated with the facilitation and competition interactions

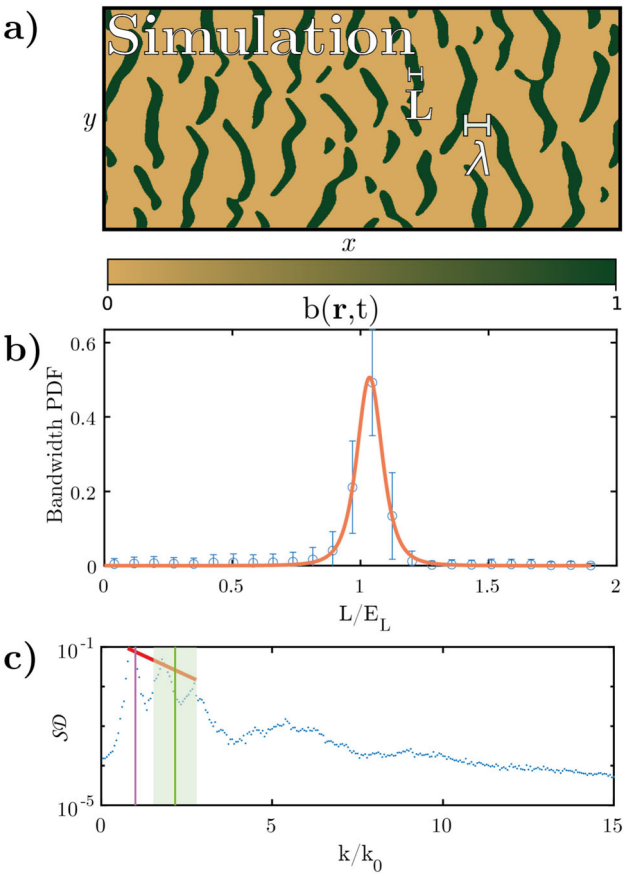

Fig. 7 Numerical intermediate regular banded vegetation patterns and their statistical characterization obtained from model Eq. (1) with $\mu = 0.9, D = 0.01, \chi_f = \chi_c = 3, l_{fx} = 1, l_{fy} = 1, l_{cx} = 30, l_{cy} = 4, \mathbf{d}_f = (0.8, 0)$, and $\mathbf{d}_c = (-2, 0)$. (**a**) Colormap of the binarized simulated biomass $b(\mathbf{r}, t)$. (**b**) Histogram of the bandwidths projected along the average direction of the pattern. Blue dots represent the frequency of the simulated bandwidth. Orange curves correspond to q-Gaussian fitting to the bandwidth distribution, with $q = 1.3$ and determination coefficient $R^2 = 0.97$. (**c**) Spectral density $\mathcal{SD}$ of the bands projected along the average direction of the pattern. The vertical green line indicates the expectation value of the bandwidth L. The shadowed green regions account for the width variance. The vertical purple line accounts for the pattern average wavelength λ

the origin of the kernel functions. The origin now is positioned at $\mathbf{d}_i = (a_i, b_i)$ as shown in Fig. 6(b). Thus, the kernel functions associated with both non-local facilitative and competitive interactions are anisotropic due to the environmental conditions, i.e., $\mathcal{K}_i(\mathbf{r} - \mathbf{r}') \neq \mathcal{K}_i(|\mathbf{r} - \mathbf{r}'|)$. Therefore, the kernels are not reciprocal $\mathcal{K}_i(\mathbf{r}, \mathbf{r}') \neq \mathcal{K}_i(\mathbf{r}', \mathbf{r})$. Figure 6(b) schematizes the spatial ranges of non-reciprocal non-local spatial interactions.

Numerical simulations of the integro-differential Eq. (1) with anisotropic kernels [see Formula 2] show a vegetation pattern with irregular bands [see Fig. 7(a)]. The simulations are conducted in a parameter range where the banded vegetation patterns are unstable, demonstrating permanent complex behavior, specifically spatiotemporal chaos [38]. All numerical simulations are carried out employing a pseudo-spectral integration scheme with a 1024×1024 grid and periodical boundary conditions. The corresponding probability density distribution of bandwidth, which represents the frequency distribution of the different bandwidths, corresponds to a q-Gaussian distribution with $q \approx 1.5$ [see Fig. 7(b)]. Then, we compute the spectral density $\mathcal{SD}$ of the biomass b, along the average direction of the irregular pattern. Figure 7(c) shows the computed spectral density. The multiple peaks in this chart indicate that the model is more regular than the field observations, but the intensity of the first three main modes also decreases as an exponential law of exponent $m = 0.92$. This spectral density shows evidence of a exponential-law decay at large wavenumber, i.e., sub-wavelength. Hence, the origin of this type of power law arises from the differences in the shapes of the bands. All the results obtained by the numerical simulations of Eq. (1) are in qualitative agreement with remote sensing image analysis.

4 Conclusions

We have analyzed several intermediate regular banded vegetation patterns in semi-arid and arid landscapes around the world. By recovering the distribution of the pattern bandwidth, we showed that the spatial irregularities can be statistically described by the q-Gaussian distribution. The computed spectral density of the vegetation patterns presents an exponential-law decay, while the biomass orientation field is shown to exhibit a power-law decay. Both decays can be

observed in the sub-wavelength regime. We have observed that deviations from the Gaussian distribution may explain why the irregularities that we observe in the spatial structure of the pattern is deterministic rather than random fluctuations. The q-statistics can serve as an early warning sight of ecological stress, such as desertification or human cause of disturbance.

The findings presented above were obtained by remote sensing image analysis. In order to investigate the spatial irregularity theoretically, a fully deterministic model, the interaction-redistribution model, was employed, in which non-local competition and facilitation, non-reciprocal interactions between plants, were taken into account. Numerical simulations in the spatiotemporal chaos regime were conducted to reproduce the observed phenomena, with similar exponents. It is noteworthy that local models are unable to reproduce these observations due to the presence of a single wavenumber. Because of the limitation of the dynamics around this characteristic wavelength, patterns have a well-defined bandwidth, and complex behaviors can only be found in the large wavelength regime.

Our theoretical approach is entirely deterministic, without relying on stochastic fluctuations or external spatial heterogeneity. However, it generates pronounced spatial irregularities, indicating that deterministic chaos, induced by non-reciprocal and non-local plant interactions, may be sufficient to explain spatial complexity in the banded vegetation patterns observed in many arid and semi-arid landscapes. Our findings clearly indicate that the irregularities present in the banded vegetation patterns are governed by well-defined statistical laws that are independent of the type of plant or soil. We can expect that, due to its general nature, the spatial irregularity shown in the pattern of vegetation bands and the statistical law governing their formation will be observed in many non-equilibrium physical systems.

Supplementary information

Supplementary movie: Time series of the numerical irregular banded vegetation patterns obtained from the interaction redistribution model with $\mu = 0.9$, $D = 0.01$, $\chi_f = \chi_c = 3$, $l_{fx} = 1$, $l_{fy} = 1$, $l_{cx} = 30$, $l_{cy} = 4$, $\mathbf{d}_f = (0.8, 0)$, and $\mathbf{d}_c = (-2, 0)$.

Appendix A Image treatment

The images were obtained from Google Earth [42] in greyscale using the "save image" tool. The highest available resolution was selected (8192 x 7016 pixels). The spatial extent of each image was chosen by visual inspection, ensuring that a complete pattern with a well-defined orientation along the x direction was captured entirely in the image (Fig. 8).

Subsequently, the images were processed with Fiji [50]. A Gaussian blur filter is applied to reduce local inhomogeneities. To analyze the bandwidths and orientation field, a subtract background algorithm was used, and then the images were binarized using the default *IsoData* algorithm, allowing the band shapes to be extracted. Small, noisy patches with an approximate radius below three pixels were removed. All these steps were carried out using prebuilt Fiji functions.

Note that, to obtain a representative bandwidth distribution, it is important to have a good image resolution. If not, the distributions are expected to be a simple peak at the expected bandwidth value. Different binarization thresholds were tested, only lightly affecting the expected value for the bandwidths and the number and size of the noisy patches.

Appendix B Bandwidth distribution

The Tsallis q-Gaussian distribution could potentially be a valuable addition to the existing statistical toolkit [39]. It offers a generalization of the classical Gaussian (or normal) distribution. The probability density function of a q-Gaussian is given by $f_q(x) = Ce_q(-\beta x^2)$ with $e_q(x)$ is the q-exponential defined as $e_q(x) = [1 + (1-q)x]^{\frac{1}{1-q}}$ and C is a normalization factor. For $q = 1$, the q-Gaussian distribution is equivalent to a classical Gaussian distribution. For $1 < q < 3$, the distribution has heavier tails, making it the ideal choice for modeling phenomena with extreme fluctuations. Observe that the tails of the distribution follow a power law decay $x^{-2/(q-1)}$.

To fit the probability density function, only positive values of bandwidths were taken into account; therefore, the fitting function reads as

$$f_q(L) = \begin{cases} A\left[1-(1-q)\beta(x-\mu)^2\right]^{\frac{1}{1-q}}, & x \geq 0, \\ 0, & x < 0. \end{cases} \quad \text{(B1)}$$

where L is the bandwidth, β, q,μ are fitting parameters, and A is the propper normalization. The fitting procedure was performed using the *Nonlinear Least Squares* method. At the same time, the bandwidths were extracted using a *Run-Length* algorithm along the x axis of the binarized images, considering only runs larger than 1 pixel. Combined with the preceding image-processing steps, this approach ensures robustness against noise and finite-size effects.

We also checked for other distributions that extend only over the positive real axis, such as the gamma and Weibull distributions. Figure 9 shows the q-Gaussian, gamma, and Weibull fits for the bandwidth distribution of the remote images.

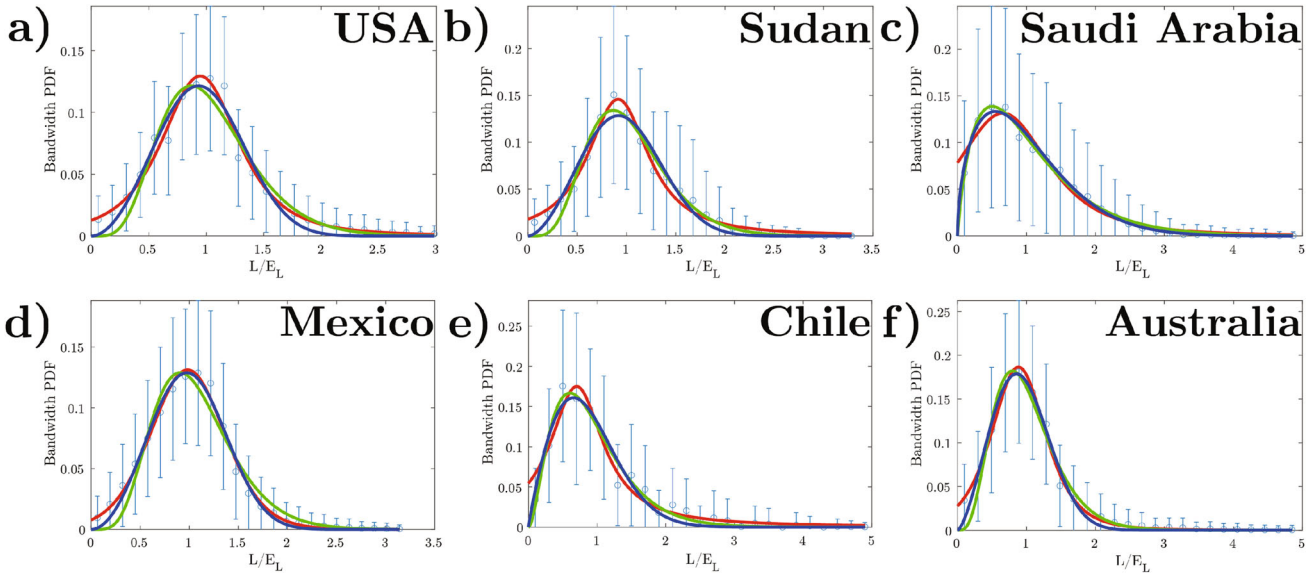

Fig. 8 Bandwidth distributions: (**a**) USA (031°02'30.00"N 103°05'30.00"W), (**b**) Sudan (011°09'00.00"N 028°16'30.00"E), (**c**) Saudi Arabia (024°19'48.00"N 042°55'12.00"E), (**d**) Mexico (028°08'30.00"N 104°28'00.00"W), (**e**) Chile (020°29'30.00"S 070°03'30.00"W), and (**f**) Australia (023°23'41.67"S 133°22'53.99"E). Red, green, and blue lines indicate q-Gaussian, gamma and Weibull distribution fits. Blue dots account for the mean probability of the bandwidth. Error bars account for the standard deviation

Overall, the q-Gaussian distribution seems to be the most adequate for the bandwidths. Figure 9 shows a comparison of the skewness and kurtosis errors for the q-Gaussian, gamma, and Weibull distributions of bandwidths in every analyzed region. As it is clearly shown, the q-Gaussian distribution usually has a smaller error for the skewness and for the kurtosis, indicating that this distribution better fits the asymmetry and the tails of the bandwidths.

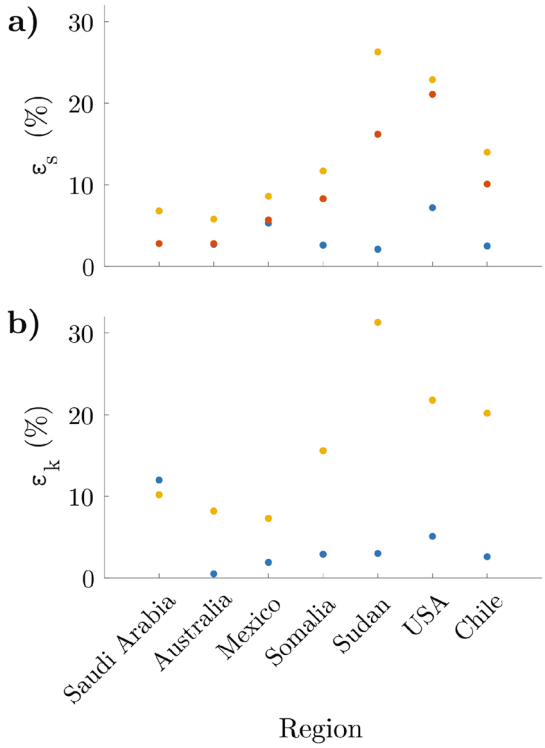

Fig. 9 Skewness and kurtosis percentual errors for the different fits. Blue, orange, and yellow points account for the q-Gaussian, gamma, and Weibull distributions, respectively

Appendix C Pattern orientation field

From the spectral density analysis, one can conclude that a single mode with a wavenumber k_0 dominates the spatial distribution of the pattern. Hence, we can define a local wave vector $\mathbf{k}(\mathbf{r})$ and its corresponding pattern orientation phase $\varphi(\mathbf{r})$ with respect to the horizontal direction [46]. We use a local approximation of the biomass field of the form $u(\mathbf{r}) \approx \mathbf{A}\cos[\varphi(\mathbf{r})]$ where A and φ are the amplitude and phase. The associated local wave vector is defined as $\mathbf{k}(\mathbf{r}) \equiv \nabla\varphi(\mathbf{r})$. It is then possible to build the pattern orientation field $\Phi(\mathbf{r}) = \arctan[\mathbf{k_y}(\mathbf{r})/\mathbf{k_x}(\mathbf{r})]$, being the angle of the wave vector with respect to a given direction (here, the horizontal one). To soften the orientational field, a Gaussian filter of parameter $\sigma_0 = 2\pi/k_0$ is applied.

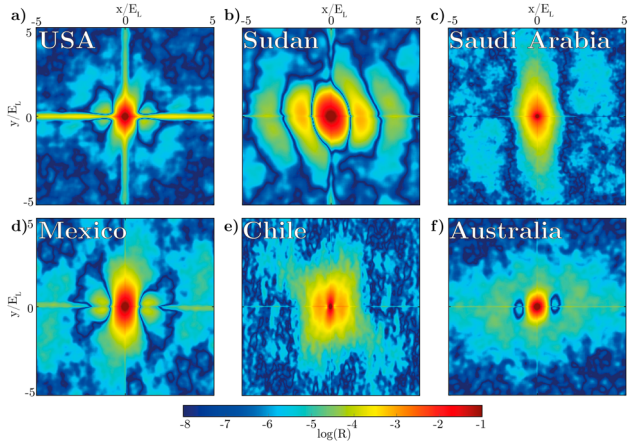

Fig. 10 Correlogram R in logarithmic scale of banded vegetation patterns in four continents: (a) USA (031°02'30.00"N 103°05'30.00"W), (b) Sudan (011°09'00.00"N 028°16'30.00"E), (c) Saudi Arabia (024°19'48.00"N 042°55'12.00"E), (d) Mexico (028°08'30.00"N 104°28'00.00"W), (e) Chile (020°29'30.00"S 070°03'30.00"W), and (f) Australia (023°23'41.67"S 133°22'53.99"E)

Appendix D Numerical integration of the interaction redistribution model

To solve model Eq. (1), we discretize the space by using a finite difference method with a spatial step of $\Delta x = 1$ in a square grid of 1024×1024 with periodic boundary conditions. The equation is numerically integrated in time with the Dormand–Prince time integrator. Random initial conditions were used (random pixels picked in a uniform distribution between 0 and 1), and the system was evolved 2500 time units, until a qualitative equilibrium was reached (Fig. 10).

Appendix E Pattern correlation

To get insight about the regularity in the different directions, one can compute the correlogram $R = \mathcal{F}^{-1}[|\mathcal{F}[b - \bar{b}]|^2]$ [7]. Figure 10 shows the correlogram of the places under study on a logarithmic scale. This is an estimation of the autocorrelation function that deviates due to the finite spatial extent. By itself, these quantities give information about the degree of similarity of a pattern with a copy of itself with a spatial translation [7]. In a periodic system, the correlation it is expected to oscillate in the characteristic direction of the periodic pattern.

Due to the complexity and irregularities in the pattern, the correlation observed in Fig. 10 presents only a couple of oscillations and then decays without further oscillations. The direction of the oscillations also presents some curvature, due to the fact that the pattern orientation is irregular and complex in space, as shown by the orientation field.

Supplementary Information The online version contains supplementary material available at https://doi.org/10.1007/s11071-025-11996-2.

Author Contributions E. A. D.-M. discussed and performed research, analyzed data, conducted numerical simulations, designed figures, and edited the manuscript. B. H.-O. discussed research, conducted numerical simulations, and edited the manuscript. M. G. C. designed and discussed research. Edited the manuscript. M. T. discussed research, wrote the paper and edited the manuscript.

Funding This work was supported by the ANID Millennium Science Initiative Program (Grant No. ICN17_012, MIRO), FONDECYT, Chile (Project No. 1210353), and Wallonie Bruxelles International (WBI). M.T. is supported by the Fonds National de la Recherche Scientifique (Belgium).

Data Availability No datasets were generated or analysed during the current study.

Declarations

Competing Interests The authors declare that there is no Conflict of interest.

References

1. Clos-Arceduc, M.: Etude sur photographies aériennes d'une formation végétale sahélienne: la brousse tigrée. Bulletin de l'IFAN Serie A **18**, 678–684 (1956)
2. Lefever, R., Lejeune, O.: On the origin of tiger bush. Bull. Math. Biol. **59**, 263–294 (1997)
3. Klausmeier, C.A.: Regular and irregular patterns in semiarid vegetation. Science **284**(5421), 1826–1828 (1999)
4. Tlidi, M., Lefever, R., Vladimirov, A.: On vegetation clustering, localized bare soil spots and fairy circles. Lect. Notes Phys. **751**, 381 (2008)
5. HilleRisLambers, R., Rietkerk, M., Van Den Bosch, F., Prins, H.H., De Kroon, H.: Vegetation pattern formation in semi-arid grazing systems. Ecology **82**(1), 50–61 (2001)
6. Hardenberg, J., Meron, E., Shachak, M., Zarmi, Y.: Diversity of vegetation patterns and desertification. Phys. Rev. Lett. **87**(19), 198101 (2001)
7. Kästner, K., van de Vijsel, R.C., Caviedes-Voullième, D., Frechen, N.T., Hinz, C.: Unravelling the spatial structure of regular dryland vegetation patterns. CATENA **247**, 108442 (2024)
8. Kästner, K., van de Vijsel, R.C., Caviedes-Voullième, D., Hinz, C.: A scale-invariant method for quantifying the regularity of environmental spatial patterns. Ecol. Complex. **60**, 101104 (2024)
9. Kästner, K., Caviedes-Voullième, D., Hinz, C.: Formation of spatial vegetation patterns in heterogeneous environments. PLoS One **20**(5), 0324181 (2025)
10. Fruchart, M., Hanai, R., Littlewood, P.B., Vitelli, V.: Nonreciprocal phase transitions. Nature **592**(5692), 363–369 (2021)
11. Alekseeva, L., Povkh, I., Stroganov, V., Kidyarov, B., Pasko, P.: A nonreciprocal optical element. J. Opt. Technol. **70**(7), 525–526 (2003)
12. Mirza, I.M., Ge, W., Jing, H.: Optical nonreciprocity and slow light in coupled spinning optomechanical resonators. Opt. Express **27**(18), 25515–25530 (2019)
13. Yang, P., Xia, X., He, H., Li, S., Han, X., Zhang, P., Li, G., Zhang, P., Xu, J., Yang, Y.: Realization of nonlinear optical nonreciproc-

ity on a few-photon level based on atoms strongly coupled to an asymmetric cavity. Phys. Rev. Lett. **123**(23), 233604 (2019)
14. Reisenbauer, M., Rudolph, H., Egyed, L., Hornberger, K., Zasedatelev, A.V., Abuzarli, M., Stickler, B.A., Delić, U.: Non-hermitian dynamics and non-reciprocity of optically coupled nanoparticles. Nat. Phys. **20**(10), 1629–1635 (2024)
15. Fleury, R., Sounas, D.L., Sieck, C.F., Haberman, M.R., Alù, A.: Sound isolation and giant linear nonreciprocity in a compact acoustic circulator. Science **343**(6170), 516–519 (2014)
16. Coulais, C., Sounas, D., Alu, A.: Static non-reciprocity in mechanical metamaterials. Nature **542**(7642), 461–464 (2017)
17. Jin, L., Khajehtourian, R., Mueller, J., Rafsanjani, A., Tournat, V., Bertoldi, K., Kochmann, D.M.: Guided transition waves in multistable mechanical metamaterials. Proc. Natl. Acad. Sci. **117**(5), 2319–2325 (2020)
18. Aguilera-Rojas, P.J., Alfaro-Bittner, K., Clerc, M.G., Díaz-Zúñiga, M., Moya, A., Pinto-Ramos, D., Rojas, R.G.: Nonlinear wave propagation in a bistable optical chain with nonreciprocal coupling. Commun. Phys. **7**(1), 195 (2024)
19. Hidalgo-Ogalde, B., Pinto-Ramos, D., Clerc, M.G., Tlidi, M.: Nonreciprocal feedback induces migrating oblique and horizontal banded vegetation patterns in hyperarid landscapes. Sci. Rep. **14**(1), 14635 (2024)
20. Cheng, Y., Stieglitz, M., Turk, G., Engel, V.: Effects of anisotropy on pattern formation in wetland ecosystems. Geophys. Res. Lett. **38**(4) (2011)
21. Mauchamp, A., Rambal, S., Lepart, J.: Simulating the dynamics of a vegetation mosaic: a spatialized functional model. Ecol. Model. **71**(1–3), 107–130 (1994)
22. Sherratt, J.A.: Using wavelength and slope to infer the historical origin of semiarid vegetation bands. Proc. Natl. Acad. Sci. **112**(14), 4202–4207 (2015)
23. Deblauwe, V., Couteron, P., Lejeune, O., Bogaert, J., Barbier, N.: Environmental modulation of self-organized periodic vegetation patterns in Sudan. Ecography **34**(6), 990–1001 (2011)
24. D'Odorico, P., Laio, F., Ridolfi, L.: Patterns as indicators of productivity enhancement by facilitation and competition in dryland vegetation. J. Geophys. Res. Biogeosci.**111**(G3) (2006)
25. Ridolfi, L., D'Odorico, P., Laio, F.: Noise-Induced Phenomena in the Environmental Sciences. Cambridge University Press, Cambridge (2011)
26. Horsthemke, W., Lefever, R.: Noise-Induced Transitions: Theory and Applications in Physics, Chemistry, and Biology. Springer, Berlin (1984)
27. García-Ojalvo, J., Sancho, J.: Noise in Spatially Extended Systems. Springer, Berlin (2012)
28. van de Koppel, J., Rietkerk, M., Van Langevelde, F., Kumar, L., Klausmeier, C.A., Fryxell, J.M., Hearne, J.W., van Andel, J.: de Ridder, N., Skidmore, A., others.: Spatial heterogeneity and irreversible vegetation change in semiarid grazing systems. The American Naturalist 159(2), 209–218 (2002)
29. Pueyo, Y., Kéfi, S., Alados, C.L., Rietkerk, M.: Dispersal strategies and spatial organization of vegetation in arid ecosystems. Oikos **117**(10), 1522–1532 (2008)
30. Thompson, S., Katul, G.: Secondary seed dispersal and its role in landscape organization. Geophys. Res. Lett. **36**(2) (2009)
31. McGrath, G.S., Paik, K., Hinz, C.: Microtopography alters self-organized vegetation patterns in water-limited ecosystems. J. Geophys. Res. Biogeosci.**117**(G3) (2012)
32. Gandhi, P., Werner, L., Iams, S., Gowda, K., Silber, M.: A topographic mechanism for arcing of dryland vegetation bands. J. R. Soc. Interface **15**(147), 20180508 (2018)
33. Bennett, J.JR., Sherratt, J.A.: Long-distance seed dispersal affects the resilience of banded vegetation patterns in semi-deserts. J. Theor. Biol. 481, 151–161 (2019)
34. Consolo, G., Valenti, G.: Secondary seed dispersal in the Klausmeier model of vegetation for sloped semi-arid environments. Ecol. Model. **402**, 66–75 (2019)
35. Zhang, H., Xu, W., Lei, Y., Qiao, Y.: Noise-induced vegetation transitions in the grazing ecosystem. Appl. Math. Model. **76**, 225–237 (2019)
36. Yizhaq, H., Stavi, I., Shachak, M., Bel, G.: Geodiversity increases ecosystem durability to prolonged droughts. Ecol. Complex. **31**, 96–103 (2017)
37. Couteron, P.: Using spectral analysis to confront distributions of individual species with an overall periodic pattern in semi-arid vegetation. Plant Ecol. **156**(2), 229–243 (2001)
38. Pinto-Ramos, D., Clerc, M.G., Tlidi, M.: Topological defects law for migrating banded vegetation patterns in arid climates. Sci. Adv. **9**(31), 6620 (2023)
39. Tsallis, C.: Possible generalization of Boltzmann–Gibbs statistics. J. Stat. Phys. **52**, 479–487 (1988)
40. Tsallis, C.: Introduction to Nonextensive Statistical Mechanics: Approaching a Complex World. Springer, New York (2009)
41. Penny, G.G., Daniels, K.E., Thompson, S.E.: Local properties of patterned vegetation: quantifying endogenous and exogenous effects. Philosophical Transactions of the Royal Society A: Mathematical, Physical and Engineering Sciences **371**(2004), 20120359 (2013)
42. Google earth software (https://earth.google.com/web)
43. Meron, E.: Nonlinear Physics of Ecosystems. CRC Press, Taylor & Francis Group Boca Raton, FL, USA (2015)
44. Clerc, M.G., Gonzalez-Cortes, G., Odent, V., Wilson, M.: Optical textures: characterizing spatiotemporal chaos. Opt. Express **24**(14), 15478–15485 (2016)
45. Liu, Z., Ouali, M., Coulibaly, S., Clerc, M., Taki, M., Tlidi, M.: Characterization of spatiotemporal chaos in a Kerr optical frequency comb and in all fiber cavities. Opt. Lett. **42**(6), 1063–1066 (2017)
46. Egolf, D.A., Melnikov, I.V., Bodenschatz, E.: Importance of local pattern properties in spiral defect chaos. Phys. Rev. Lett. **80**(15), 3228 (1998)
47. Bernd, J.: The problem of vegetation stripes in semi-arid Africa. Plant Res. Dev **8**, 37–50 (1978)
48. Patchiness in vegetation in the northern sudan: G.A., W. J. Ecol. **48**, 107–115 (1960)
49. White, L.P.: Vegetation arcs in Jordan. J. Ecol. **57**, 461–464 (1969)
50. Schindelin, J., Arganda-Carreras, I., Frise, E., Kaynig, V., Longair, M., Pietzsch, T., Preibisch, S., Rueden, C., Saalfeld, S., Schmid, B.: Fiji: an open-source platform for biological-image analysis. Nat. Methods **9**(7), 676–682 (2012)